Applied Catalysis A: General 486 (2014) 49–54

Contents lists available at ScienceDirect

Applied Catalysis A: General

journal homepage: www.elsevier.com/locate/apcata

In situ studies of structural changes in DME synthesis catalyst with synchrotron powder diffraction

Kazi Bayzid Kabir[a], Helen E. Maynard-Casely[b,1], Sankar Bhattacharya[a,*]

[a] Department of Chemical Engineering, Monash University, Clayton, Victoria -3800, Australia
[b] Australian Synchrotron, 800 Blackburn Road, Clayton, Victoria -3168, Australia

ARTICLE INFO

Article history:
Received 22 June 2014
Received in revised form 14 August 2014
Accepted 22 August 2014
Available online 29 August 2014

Keywords:
Dimethyl ether
Bi-functional catalyst
Synchrotron radiation
X-ray diffraction
Structural changes

ABSTRACT

Structural changes in a bi-functional dimethyl ether synthesis catalyst (CuO-ZnO-Al_2O_3-MgO + γ-Al_2O_3, BFC), a methanol synthesis catalyst (CuO-ZnO-Al_2O_3-MgO, MSC) and a methanol dehydration catalyst (γ-Al_2O_3, MDC), were studied using X-ray synchrotron powder diffraction. The catalysts were first reduced in 10% H_2/He and then treated in a gas containing CO, H_2 and CO_2. Measurements were taken at temperatures between 50 °C and 500 °C. These measurements were complemented by ex-situ techniques—thermogravimetry (TG) and scanning electron microscopy (SEM)/energy-dispersive X-ray spectroscopy (EDS). The X-ray diffraction (XRD) results showed that the copper oxide phase, present in methanol synthesis and bi-functional catalysts, reduced to form Cu^0 after reduction. No further chemical changes were observed for these catalysts. γ-Al_2O_3 was resistant to structural and chemical changes. The copper crystallite sizes of the methanol and bi-functional catalysts were found to increase with temperature. The extent of deactivation was higher for CuO-ZnO-Al_2O_3-MgO + γ-Al_2O_3 compared to CuO-ZnO-Al_2O_3-MgO.

© 2014 Elsevier B.V. All rights reserved.

1. Introduction

Single-step conversion of syngas to dimethyl ether (DME) has received significant attention in the synthetic fuel research area since 1991 [1]. Conventional two-step synthesis involves production of methanol from syngas, purification of methanol and then dehydration of methanol in a separate reactor to produce DME. The single-step process eliminates the intermediate step, by incorporating both the reactions in the same reactor. This process also has higher yield than the conventional process, since it removes the thermodynamic limitation of CO-hydrogenation [2] by in situ dehydration of methanol to DME. A hydrogenation catalyst (usually copper based [2]) and a dehydration catalyst (usually γ-Al_2O_3 [3]) placed in a single reactor are responsible for one-step conversion of syngas to DME. Copper-based catalysts have various industrial applications (i.e. methanol synthesis, water-gas shift, methanol reforming) and hence extensively studied over the years [4–9]. Meanwhile, a wide range of solid acids (e.g. alumina, silica-alumina, zeolites) have also been studied as methanol dehydration catalyst [10]. A combination of these two catalysts, usually called a bi-functional catalyst [11], is a relatively new concept and merits extensive investigation for optimal integration of the two conventional steps.

The properties of the catalyst under reaction conditions can be different from ambient conditions. Therefore, ex situ characterisation of catalysts does not always provide useful data on how the catalyst would perform in realistic reaction conditions. The high-flux of synchrotron based radiation sources (10^1 to 10^{10} times brighter than conventional laboratory X-ray sources [12]) enables the study of solid catalysts in situ within high-pressure and high-temperature environment [13].

Advantageous features of synchrotron radiation (SR), such as beam stability and continuous tunability, have resulted in immense progress in the application of SR based techniques for catalyst characterisation over the past 20 years [12]. Combination of different techniques also enables acquisition of complementary data from the same set of experiments. Conversion of aurichalcite precursor to copper catalyst (for reverse water gas shift) was studied by recording diffraction and absorption sequentially with a very short time delay [14]. Time-resolved XRD was combined with Raman and mass spectroscopy to investigate the behaviour of SAPO-34 under methanol-to-olefin (MTO) condition [15]. XRD identified the chemical and structural changes in the catalyst. The nature of coke formed during the MTO condition was observed in the Raman

---

[*] Corresponding author.
E-mail address: sankar.bhattacharya@monash.edu (S. Bhattacharya).
[1] Current address: Bragg Institute, Australian Nuclear Science and Technology Organisation, Kirrawee DC, NSW-2232, Australia.

http://dx.doi.org/10.1016/j.apcata.2014.08.027
0926-860X/© 2014 Elsevier B.V. All rights reserved.

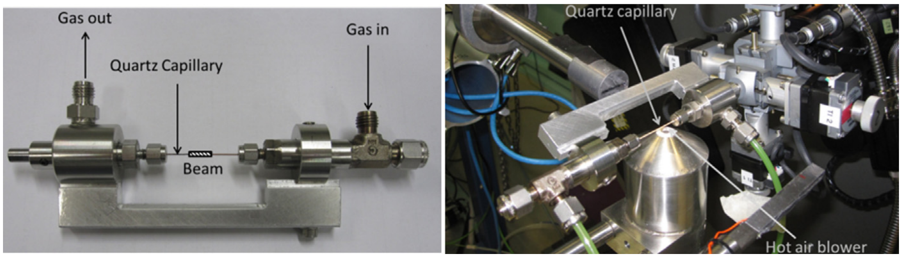

Fig. 1. (a) Flow cell with sample inside the quartz capillary, (b) flow cell-hot air blower configuration.

Table 1
Bulk composition of the MSC and MDC catalysts (wt%).

	CuO	ZnO	Al_2O_3	MgO	C
CuO-ZnO-Al_2O_3-MgO	63.6	24.8	10.3	1.30	–
γ-Al_2O_3	–	–	96.5	–	3.50

spectra while mass spectra provided information regarding the gaseous product [15]. XRD study of hydrothermally synthesised nickel succinate was also studied for dehydration–rehydration (40–200 °C) and decomposition (up to 600 °C) [16].

Changes in phase structures of binary (Cu, Zn) and ternary (Cu, Zn, Al) catalysts were studied in situ using a reactor-X-ray powder diffraction (XRD) cell during activation and synthesis conditions [17]. The CuO phase present in the catalyst reduced to Cu^0. The activity also steadily decreased with on-stream time. This investigation was further developed using a combination of XRD and X-ray absorption fine structure spectroscopy (XAFS) [18]. Alloying of Cu and Zn was observed when the catalysts were heated to 300 °C or above.

The focus of the current study is on dimethyl ether synthesis catalyst. Study on the effect of the addition of the dehydration component to the methanol synthesis catalyst using in situ techniques has not been reported in the literature. Therefore, in this study dynamic changes in the structure of the bi-functional catalyst for DME synthesis during activation and synthesis reaction were investigated using in situ synchrotron XRD. Studies only on the methanol synthesis catalyst and dehydration catalyst were also performed to examine the effect of the dehydration component on the performance of methanol synthesis catalyst. Complementary analysis was undertaken using thermogravimetry (TG) and scanning electron microscopy (SEM) with energy dispersive X-ray spectroscopy (EDS).

2. Materials and methods

2.1. Materials

A commercial methanol synthesis catalyst (CuO-ZnO-Al_2O_3-MgO) and a commercial methanol dehydration catalyst (γ-Al_2O_3), were used in the current study. The samples will be called MSC and MDC from here onwards. Bulk compositions of the catalysts are shown in Table 1. The bi-functional catalyst for syngas to DME synthesis was prepared by physically mixing the commercial catalysts. The ratio of the MSC to MDC in the bi-functional catalyst was 3–1 (mass basis). Two gas mixtures (10% H_2 in He; CO 40%, H_2 40% and CO_2 20%) were also used during the XRD measurements.

2.2. Methods

The catalysts were studied by the powder diffraction beam line end station (10-BM-1) at the Australian Synchrotron [19,20]. In a typical experiment, ca. 50 mg of catalyst was loaded into 0.7 mm OD (0.5 mm ID) quartz capillary. The catalyst loaded quartz capillary was then inserted into the flow cell, as shown in Fig. 1 (a). The flow cell was then installed on to the beamline end station, as shown in Fig. 1(b). The beam size at the sample was 1 mm (horizontal) × 1.2 mm (vertical). The beam was focused at the centre of the quartz capillary. The catalyst was reduced by flowing 10% H_2 in He gas through the flow cell from room temperature to 250 °C using a gas manifold. The sample holder and the flow cell were allowed to oscillate by 10 degrees to ensure maximum interaction between the bulk sample and the X-ray source. A Cyberstar hot air blower was used to heat up the sample inside the capillary at a heating rate of 10 °C/min. Diffraction patterns from the capillary were collected with the MYTHEN-II strip detector [21] at a wavelength of 0.7743 Å (approximately 16,000 keV). The wavelength was determined from the refinement of a NIST LaB_6-660b standard. Before collecting the diffraction patterns the catalyst was held at a given temperature for 20 min. At 250 °C the gas was changed from H_2-He mixture to CO-H_2-CO_2 mixture. Fig. 2 shows the temperature profile and times for the 12 diffraction spectra collected during the course of the experiment. Each diffractogram was collected for 10 min. No further analysis of the exhaust gas from the flow cell was performed.

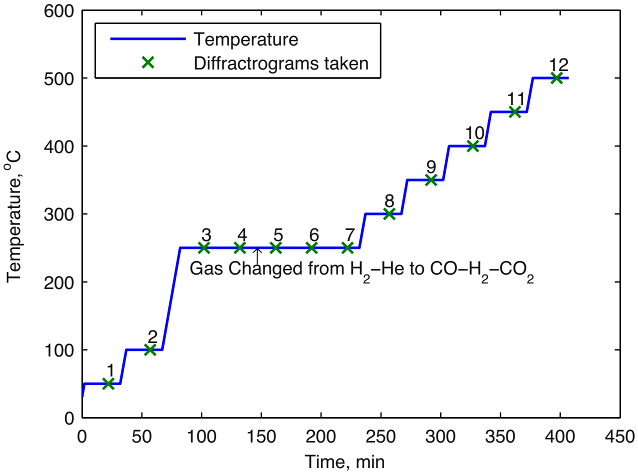

Fig. 2. Temperature profile for XRD measurements (measurement times are indicated by x).

Structural parameters of the crystalline copper were obtained after Reitveld refinement of the XRD data using TOPAS [22]. Copper crystallite size in (1 1 1) direction was calculated using the Scherrer equation [23]:

$$L = \frac{K\lambda}{B\cos\theta}$$

where B is the full width at half maximum (FWHM) of the peak profile, L is the volume average of crystal thickness in direction normal to the reflection plane, K is the constant of proportionality, θ is the angle of the reflection and λ is the wavelength.

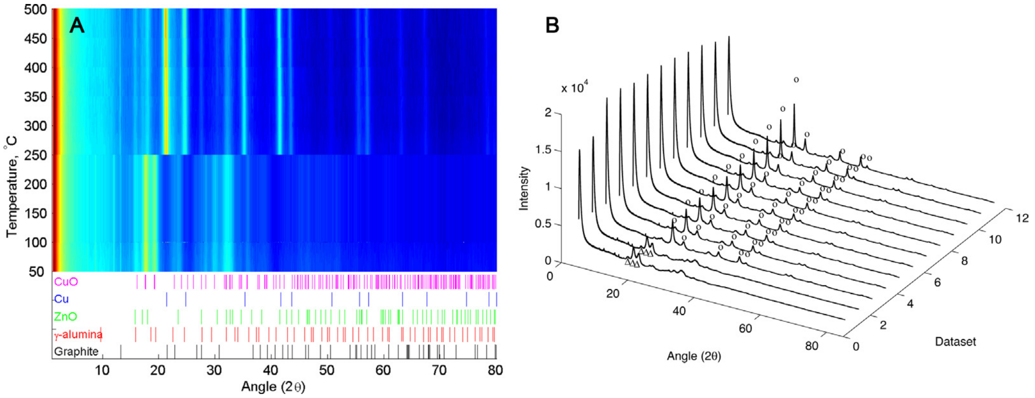

Fig. 3. Diffraction pattern for bi-functional catalyst. (a) 3D plot (only copper oxide and copper phases are shown; Δ—CuO; O—Cu). (b) 2D projection (phase reflections are shown as tick marks at the bottom of the figure).

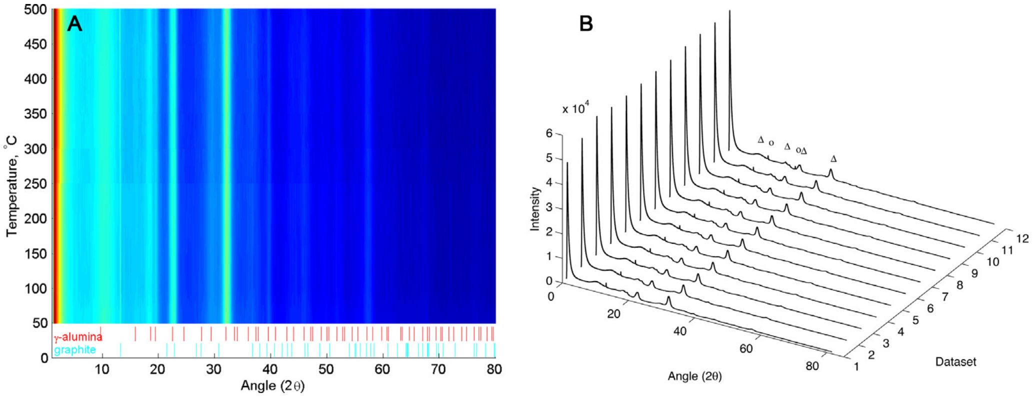

Fig. 4. Diffraction pattern for MDC. (a) 3D plot (Δ—γ-Al_2O_3; O—graphite). (b) 2D projection (phase reflections are shown as tick marks at the bottom of the figure).

The surface morphology and point compositions were studied using JEOL 7001F scanning electron microscope (SEM) equipped with energy dispersive X-ray spectrometer (EDS). Thermogravimetric analysis of the catalyst was performed using a NETZCH STA 449 F3 Jupiter® thermobalance. The analysis conditions were similar to the XRD measurements, as shown in Fig. 2.

A fixed-bed reactor (Parr 5403 continuous flow tubular reactor) was used for the conversion studies. The reactor was designed for pressures up to 34 MPa and temperatures up to 550 °C. The reactor has a brass liner to avoid methanation reaction. For determining catalyst activities, the reactor was loaded with catalyst particles between 425 and 850 μm (20–40 mesh) size. The catalyst was reduced at 190 °C (5% H_2 in nitrogen). The reactor temperature was then raised to the reaction temperature. Synthesis reaction was carried out at a space velocity of 2000 mL g_{cat}^{-1} h^{-1}. Online analysis of the outlet gas was carried out using Agilent 7890A (G3440A) GC equipped with four columns (HayeSepN, MolSieve 5A, Porapak Q and Sulfinert) and three detectors (TCD, FID and FPD).

3. Results and discussion

The bulk structure of methanol synthesis catalyst under reduction and DME synthesis conditions was studied by in situ synchrotron XRD. Bi-functional catalyst for DME synthesis was prepared by physically mixing three parts MSC and one part MDC by weight. The XRD patterns for bi-functional catalyst are shown in Fig. 3. The first diffractogram for the fresh catalyst indicates presence of CuO, ZnO, and γ-alumina. The catalyst also showed the presence of a small amount of malachite as indicated by the small peaks at lower 2θ values. In the diffraction patterns, only the peaks corresponding to Cu^0 and CuO are highlighted.

When the sample was heated to 100 °C, no structural changes were observed. As the temperature was increased to 250 °C in flowing H_2/He, the CuO was reduced to Cu^0. The reduction of copper oxide to copper is believed to be a single step process according to the following reaction:

$$CuO + H_2 \rightarrow Cu + H_2O$$

At the end of the reduction, CuO or Cu_2O phases were not detected, and only metallic phase of copper was observed.

At 250 °C, the gas was switched from H_2-He to CO-H_2-CO_2 mixture for the rest of the experiment. No new phases evolved during the course of the reaction. However, the copper peak intensities gradually increased with longer exposure of the catalyst to the synthesis gas at 250 °C or higher temperatures. The crystalline graphite phase showed directional growth on plane (1 0 0) at $2\theta = 21.4°$ and plane (2 2 1) at $2\theta = 30.8°$. These peaks indicate the coke formation by condensation of the hydrocarbons on the catalyst surface at higher temperatures.

The XRD patterns for the MSC catalyst showed similar phase changes as the bi-functional catalyst at different temperatures. Hence, the spectrogram is not shown here.

Diffraction patterns for MDC are shown in Fig. 4. The catalyst is composed of amorphous γ-Al_2O_3 with small amount of carbon (Rhombohedral graphite). The XRD pattern did not show any change in the crystalline phase of the γ-Al_2O_3 during the experiment. However, directional growth of the graphite phase, similar to that of BFC, was observed. In fact, CO hydrogenation can occur on γ-Al_2O_3 surface, in absence of MSC-1. The CO conversion is

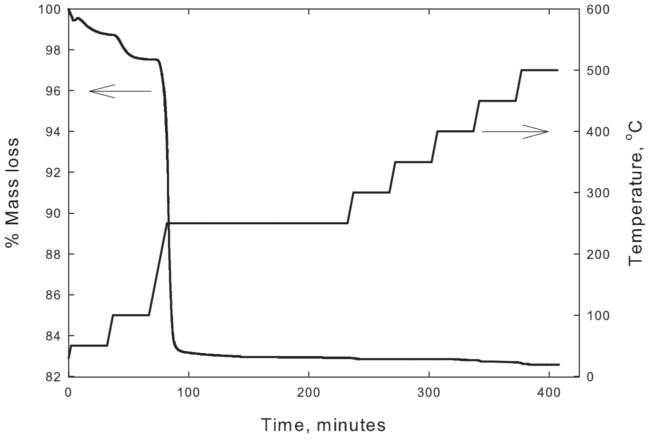

Fig. 5. Thermogravimetric analysis of the bi-functional catalyst.

Table 2
Summary of Rietveld refinement.

Temperature	Methanol synthesis catalyst		Bi-functional catalyst	
	G	R_{exp}	*G*	R_{exp}
250	2.585	4.009	2.576	4.236
300	2.491	4.076	2.586	4.26
350	2.496	4.166	2.584	4.285
400	2.657	4.261	2.617	4.272
450	2.839	4.29	2.714	4.227
500	3.061	4.28	2.75	4.191

usually low and the products are predominantly hydrocarbons [24]. Coke formation on the surface occurs by condensation of these hydrocarbons on the surface [25].

The XRD patterns for all three samples also showed the presence of structures below the XRD cutoff, which is usually less than 2–3 nm [26]. The presence of nano-crystallites (particles below XRD cutoff) is indicated by the first peak in each XRD, at approximately 2θ of 2, indicated by the red pattern in Figs. 3(a) and 4(a).

A complementary thermogravimetric analysis was performed on the bi-functional catalyst under the same conditions as the in situ XRD studies. The results are plotted in Fig. 5. The catalyst was heated from room temperature in a 5% H_2 in He environment. The sample was heated to 100 °C and held at 100 °C for 30 min. At this temperature, the sample lost approximately 2% mass due to moisture loss. After this holding period, the sample was heated again to 250 °C. The caralyst exhibited a sudden drop in mass from 180 °C due to the reduction of the copper oxide phase to Cu by H_2 present in the reducing gas. The reduction was completed before 250 °C beyond which there was no significant change in the mass of the sample. The TGA results complements well with XRD results, where diffraction patterns show the formation of metallic Cu peaks at 250 °C and disappearance of CuO peaks.

The XRD measurements were not continuous and only taken at temperatures shown in Fig. 2, start of the reduction could not be approximated from the XRD measurements. However, the TG curve provides both start and end temperatures for the reduction.

Total weight loss observed during the reduction step, according to the TG curve, corresponds to the loss of oxygen atom from copper oxide. No further changes in the weight were observed for the rest of the experiment.

Lattice parameters of Cu were determined using Rietveld refinement [27]. The weighted profile *R*-factor (R_{exp}) and goodness of fit (G) for the refinement is shown in Table 2. Changes in the lattice parameter for MSC and bi-functional catalyst are shown in Fig. 6. The lattice parameters increased with temperature in line with the expected thermal expansion.

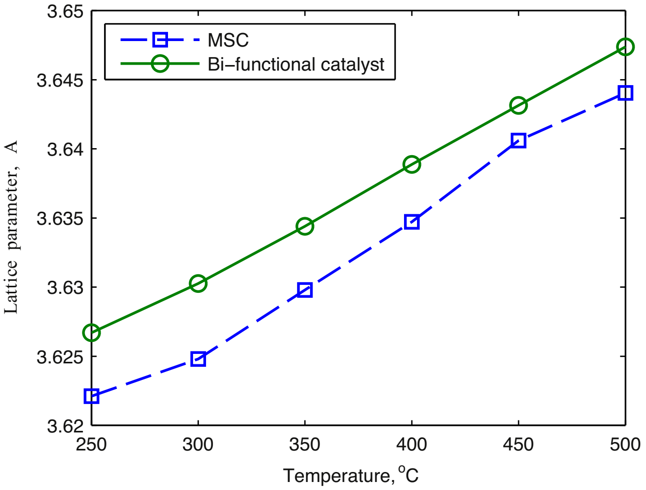

Fig. 6. Lattice parameter of Cu for MSC and bi-functional catalysts.

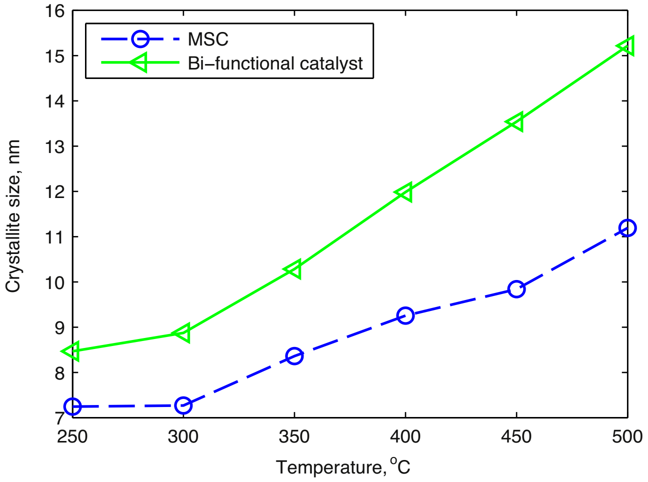

Fig. 7. Variation of copper crystallite size in [111] direction with temperature.

Change in copper crystallite size as a function of temperature is shown in Fig. 7. For both MSC and bi-functional catalysts, size of the copper crystal increased with temperature and on-stream time. Variation in the crystal size is insignificant between 250 and 300 °C. However, rapid growth in crystal size was observed above 300 °C.

Activity of the catalyst is dependent on the crystallite size, in this instance copper. The activity of the catalyst is inversely related to the copper crystallite size. The change in the metallic Cu crystallite size as a function of temperature is shown in Fig. 7. The results show that the crystallite size of both MSC and the bi-functional catalyst on freshly reduced catalyst is 7.2 nm and 8.5 nm, respectively, at 250 °C. The introduction of syngas at 250 °C and heating up to 300 °C did not show a significant effect on the Cu-crystallite size, suggesting the stability of the catalysts in this temperature range. However, when the reaction temperature increased beyond 300 °C, the crystallite size of Cu increased rapidly and reached 11.1 nm and 14.2 nm at 500 °C for MSC-1 and bi-functional catalysts, respectively. The results suggest agglomeration of the crystallites or thermal sintering at higher temperatures. Thermal sintering occurs above the Tammann temperature of copper ($\approx 0.5T_{melting} = 409.5$ °C). Sintering by release of atomic or molecular species from crystallites can occur above the Hütting temperature of copper ($\approx 0.33T_{melting} = 182$ °C) [28]. Presence of moisture or high CO_2 in the gas phase also accelerates sintering

Table 3
Point composition of the fresh and used catalysts.

Elements	Fresh MSC				Used MSC			
	Spectrum1	Spectrum2	Spectrum3	Spectrum4	Spectrum1	Spectrum2	Spectrum3	Spectrum4
Cu	47.4	47.3	48.8	48.3	36.1	36.8	38.8	33.5
Zn	24.5	24.2	25.0	23.8	24.6	24.7	24.2	26.2
Al	1.33	1.51	1.11	1.42	7.84	7.61	6.39	8.61
Mg	0.99	1.01	–	0.99	1.08	1.06	1.00	1.37
O	25.8	26.1	25.1	25.5	30.4	29.8	29.6	30.4

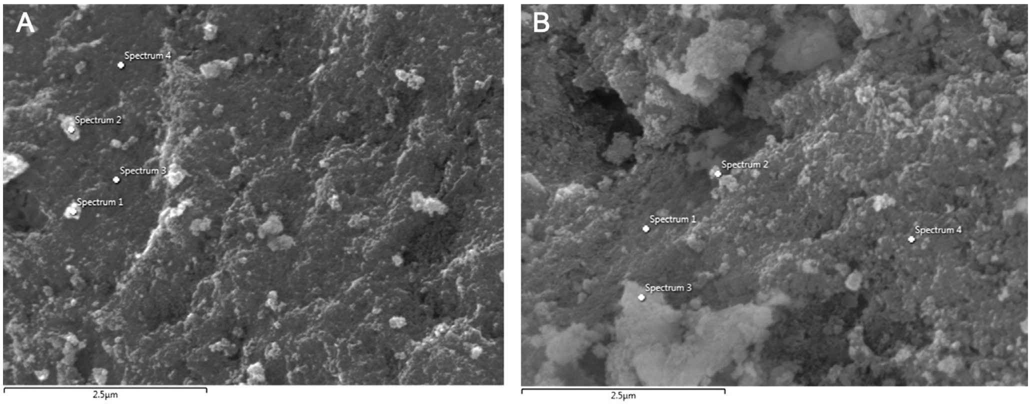

Fig. 8. Secondary electron images of the fresh (left) and used (right) catalyst.

as these gases hinder stabilisation of Cu/ZnO by the alumina phase. The crystallite sizes calculated from the XRD data clearly indicate that crystallite sizes are larger for the bi-functional catalyst. When MDC is used in conjunction with MSC for syngas to DME synthesis, the dehydration and water gas shift reaction produces H_2O and CO_2, respectively. Therefore, the extent of deactivation was greater for the bi-functional catalyst than that of the MSC.

Changes in the surface morphology for MSC are shown in Fig. 8. The catalyst before reduction showed surface morphology without any significant features. The surface was found to be nonporous. In contrast, cracks developed on the surface of the catalyst during thermal treatment in reducing environments. The point composition measurements using EDS technique for the fresh and used catalyst also showed significant changes for Cu and Al. The surface of the used catalyst is found to have more Al than the fresh catalyst, while the fresh catalyst had more copper than the used one. Zinc and magnesium concentration on the surface found to be similar for both fresh and used catalyst. The variation in surface composition is shown in Table 3. The final temperature was high enough to make the atoms or ions present in the bulk phase migrate to the surface of the catalyst. Mobility of the bulk phase therefore can be attributed to the change in the surface composition.

The DME yield and selectivity of the bi-functional catalyst at different temperatures are presented in Fig. 9. Effect of temperature on the selectivity of other product is shown in Table 4. Conversion of CO in presence of this catalyst can lead to the formation of methanol and DME (via hydrogenation reaction), methane and other hydrocarbons (methanation and Fisher-Tropsch reactions) and CO2 (through water gas shift reaction). The selectivity of the products depends on the temperature, as indicated by Fig. 9 and Table 4. At lower temperature (190 °C), the CO conversion was low (2.61%) and the oxygenate (DME + methanol) selectivity was ~99%, as the rates of methanation and water gas shift reactions were very low. At 240 °C and 300 °C, increase in the oxygenate yield can be attributed to the increase in the rates of methanol synthesis and methanol dehydration reactions. At these temperatures, copper-based catalyst also acts as a good water gas shift catalyst. Therefore, a significant increase in CO2 yield was observed which also resulted in a decrease in the oxygenate selectivity. At 340 °C, the oxygenate selectivity went further down to ~35%. This can be attributed to a combination of factors: decrease in the catalyst activity (from rapid growth in Cu crystallite size, Fig. 7), decomposition of DME into hydrocarbons in the acidic alumina sites and coke formation on the catalyst surface (observed during the X-ray diffraction measurements, Figs. 3 and 4).

Table 4
Product selectivity at various temperatures.

Products	Reaction temperature (°C)			
	190	240	290	340
DME + methanol	99.02	64.01	61.77	34.51
CO_2	0.46	35.23	35.87	45.16
CH_4 and other hydrocarbons	0.52	0.76	2.36	20.33

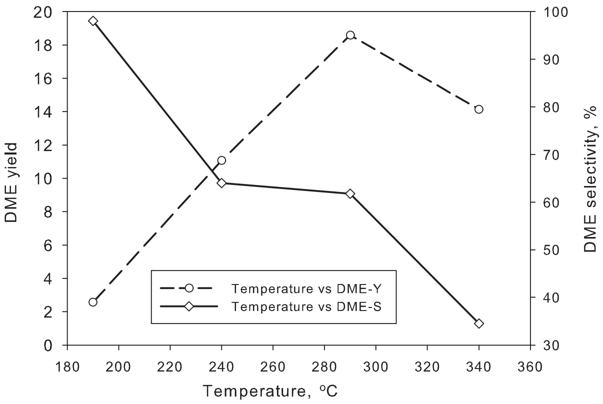

Fig. 9. DME yield and selectivity for bi-functional catalyst at different temperatures. Feed: 50% CO + 50% H_2; Pressure: 5 MPa; space velocity: 2000 mL g_{cat}^{-1} h^{-1}.

4. Conclusions

During reduction of the catalyst, MSC and bi-functional catalysts went through a chemical change in the copper oxide phase forming metallic copper. During synthesis reaction, no further chemical changes were observed. However, the crystalline copper phase grew at the expense of microstructural features of the catalyst. γ-Al_2O_3 did not show any change in the bulk structure. Copper crystallite size and its growth with temperature were higher for the bi-functional catalyst than that of the MSC indicating accelerated deactivation of the bi-functional catalyst. The deactivation can be due to the formation of water during dehydration of methanol which when adsorbed onto the alumina support aids in the growth of copper crystallites. Surface composition of the catalysts also changed during thermal treatment.

Acknowledgement

The work is supported by the Brown Coal Innovation Australia (BCIA) and the Australian Research Council (ARC) LIEF Grant. Facilities at the Australian Synchrotron (Experiment no.: AS123/PD/5266) and Monash Centre for Electron Microscopy (MCEM) were used for the current work. The authors would also like to thank Ms. Joanne Tanner, Mr. Kawnish Kirtania, Mr. Sharmen Rajendran and Dr. Srikanth Chakravartula Srivatsa for their help during different stages of the experiments.

References

[1] D.M. Brown, B.L. Bhatt, T.H. Hsiung, J.J. Lewnard, F.J. Waller, Catal. Today 8 (1991) 279–304.
[2] J.B. Hansen, P.E. Højlund Nielsen, G. Ertl, H. Knozinger, F. Schuth, J. Weitkamp (Eds.), Handbook of Heterogeneous Catalysis, 2nd ed., Wiley-VCH, Weinheim, 2008, pp. 2920–2949.
[3] A.I. Osman, J.K. Abu-Dahrieh, D.W. Rooney, S.A. Halawy, M.A. Mohamed, A. Abdelkader, Appl. Catal. B 127 (2012) 307–315.
[4] C. Ratnasamy, J.P. Wagner, Catal. Rev. 51 (2009) 325–440.
[5] S. Sá, H. Silva, L. Brandão, J.M. Sousa, A. Mendes, Appl. Catal. B 99 (2010) 43–57.
[6] K.C. Waugh, Catal. Lett. 142 (2012) 1153–1166.
[7] G.C. Chinchen, P.J. Denny, J.R. Jennings, M.S. Spencer, Appl. Catal. 36 (1988) 1–65.
[8] K. Klier, in: D.D. Eley, H. Pines, P.B. Weisz (Eds.), Advances in Catalysis, vol. 31, 1st ed., Academic Press, New York, 1982, pp. 243–313.
[9] T. Ressler, B.L. Kniep, I. Kasatkin, R. Schlögl, Angew. Chem. Int. Ed. 44 (2005) 4704–4707.
[10] J.J. Spivey, Chem. Eng. Commun. 110 (1991) 123–142.
[11] S. Bhattacharya, K.B. Kabir, K. Hein, Prog. Energ. Combust. 39 (2013) 577–605.
[12] A.M. Beale, S.D.M. Jacques, B.M. Weckhuysen, Chem. Soc. Rev. 39 (2010) 4656–4672.
[13] J.-D. Grunwaldt, B. Clausen, Top. Catal. 18 (2002) 37–43.
[14] J.W. Couves, J.M. Thomas, D. Waller, R.H. Jones, A.J. Dent, G.E. Derbyshire, G.N. Greaves, Nature 354 (1991) 465–468.
[15] D.S. Wragg, R.E. Johnson, M. Balasundaram, P. Norby, H. Fjellvåg, J. Catal. 268 (2009) 290–296.
[16] N. Guillou, C. Livage, W. van Beek, M. Noguès, G. Férey, Angew. Chem. 115 (2003) 667–671.
[17] B.S. Clausen, G. Steffensen, B. Fabius, J. Villadsen, R. Feidenhans'l, H. Topsøe, J. Catal. 132 (1991) 524–535.
[18] J.-D. Grunwaldt, A.M. Molenbroek, N.Y. Topsøe, H. Topsøe, B.S. Clausen, J. Catal. 194 (2000) 452–460.
[19] K.S. Wallwork, B.J. Kennedy, D. Wang, AIP Conf. Proc. 879 (2007) 879–882.
[20] Australian Synchrotron, Technical information (Powder), available at: https://www.synchrotron.org.au/index.php/aussyncbeamlines/powder-diffraction/technical-information (cited: 11 January 2013).
[21] A. Bergamaschi, A. Cervellino, R. Dinapoli, F. Gozzo, B. Henrich, I. Johnson, P. Kraft, A. Mozzanica, B. Schmitt, X. Shi, J. Synchrotron Radiat. 17 (2010) 653–668.
[22] Bruker AXS, TOPAS V3.0. General Profile and Structure Analysis Software for Powder Diffraction Data, Karlsruhe, Germany, 2004.
[23] E.J. Mittemeijer, U. Welzel, Z. Kristallogr. 223 (2008) 552–560.
[24] W. Zhang, H. Yang, G. Su, R. Gao, Y. Yin, Catal. Lett. 30 (1994) 113–122.
[25] Z. Sarbak, E.G. Derouane, V. Parmon, F. Lemos, F. Ramoa Ribeiro (Eds.), Sustainable Strategies for the Upgrading of Natural Gas: Fundamentals, Challenges and Opportunities, 1st ed., Springer, Dordrecht, 2005, pp. 359–364.
[26] B.S. Clausen, H. Topsøe, R. Frahm, D.D. Eley, W.O. Haag, B. Gates, H. Knözinger (Eds.), Advances in Catalysis, vol. 42, 1st ed., Academic Press, New York, 1998, pp. 315–344.
[27] L.B. McCusker, R.B. Von Dreele, D.E. Cox, D. Louer, P. Scardi, J. Appl. Crystallogr. 32 (1999) 36–50.
[28] D.L. Trimm, C.H. Bartholomew, J.B. Butt (Eds.), Catalyst Deactivation 1991: Proceedings of the 5th International Symposium, 1st ed., Elsevier, Amsterdam, 1991, pp. 29–51.